Properties of three-dimensional plasmonic slot waveguides

Georgios Veronis[1] and Shanhui Fan[2]

[1]Department of Electrical and Computer Engineering, Louisiana State University, Baton Rouge, LA 70806

[2]Department of Electrical Engineering, Stanford University, Stanford, California 94305

ABSTRACT

We investigate the properties of the modes supported by three-dimensional subwavelength plasmonic slot waveguides. We show that the fundamental mode supported by a symmetric plasmonic slot waveguide, composed of a subwavelength slot in a thin metallic film embedded in an infinite homogeneous dielectric, is always a bound mode. Its modal fields are highly confined over a wavelength range extending from zero frequency to the ultraviolet. We then show that for an asymmetric plasmonic slot waveguide, in which the surrounding dielectric media above and below the metal film are different, there always exists a cutoff wavelength above which the mode becomes leaky.

Keywords: Plasmonic devices, subwavelength optical devices, integrated optics

1. INTRODUCTION

Guiding electromagnetic waves with a mode at deep subwavelength scale is of great recent interest. In the visible wavelength range, the typical way to create a subwavelength waveguide involves the use of the so-called surface plasmon polaritons (SPPs). SPPs are bound non-radiative surface modes which propagate at metal-dielectric interfaces with field components decaying exponentially with distance away from the interface.[1] The decay length of the fields can be much smaller than the wavelength near the surface plasmon frequency. Several different plasmonic waveguiding structures have been proposed,[2–9] such as metallic nanowires,[3,4] metallic nanoparticle arrays,[5,6] and V-shaped grooves.[7,8] However, all these geometries[3–8] are fundamentally limited by the fact that they support a highly-confined mode *only* near the surface plasmon frequency. In this regime, the optical mode typically has low group velocity and short propagation length.

At microwave frequencies, where metals do not have a plasmonic response, two-conductor waveguides are used to guide subwavelength modes. Such waveguiding structures always support a fundamental TEM or quasi-TEM mode which can have deep subwavelength size and broad guiding bandwidth.[10] In addition, it has been shown that the guiding wavelength range of subwavelength modes by such structures extends into the infrared and visible wavelengths.[11] In the optical wavelength range, however, metals have a plasmonic response.[12] The properties of the optical modes supported by plasmonic two-conductor waveguides are therefore quite different from those of their counterparts at microwave frequencies, where metals behave almost as perfect electric conductors.[10] Several different plasmonic two-conductor waveguide structures have been proposed to guide light.[13–18] Because of the predicted attractive properties of plasmonic two-conductor waveguides, people have also started to explore such structures experimentally.[19,20]

Among all plasmonic two-conductor waveguides, a three-dimensional (3D) plasmonic waveguide based on a deep subwavelength slot in a thin metallic film was recently investigated.[16–18,21,22] The geometry of such a plasmonic slot waveguide is shown in Figure 1a. It consists of a slot in a thin metal film. The thin metal film is embedded in dielectric. The supported optical mode is highly localized in the slot, and its direction of propagation is parallel to the slot. Figure 1b shows a cross-sectional view of the waveguide geometry. It was shown that such a plasmonic slot waveguide supports a single fundamental mode over a wide range of frequencies.[16] The size of this mode is completely dominated by the near field of the slot, and can be far smaller than the wavelength even when the effective index of the mode approaches that of the substrate. In addition, the group velocity of the mode is close to the speed of light in the substrate, and its propagation length is tens of microns at the optical communication wavelength (λ_0 =1.55 μm). Thus, such a plasmonic slot waveguide could be potentially important in providing an interface between conventional optics and subwavelength electronic

Plasmonics: Metallic Nanostructures and Their Optical Properties VI, edited by Mark I. Stockman
Proc. of SPIE Vol. 7032, 703216, (2008) · 0277-786X/08/$18 · doi: 10.1117/12.794322

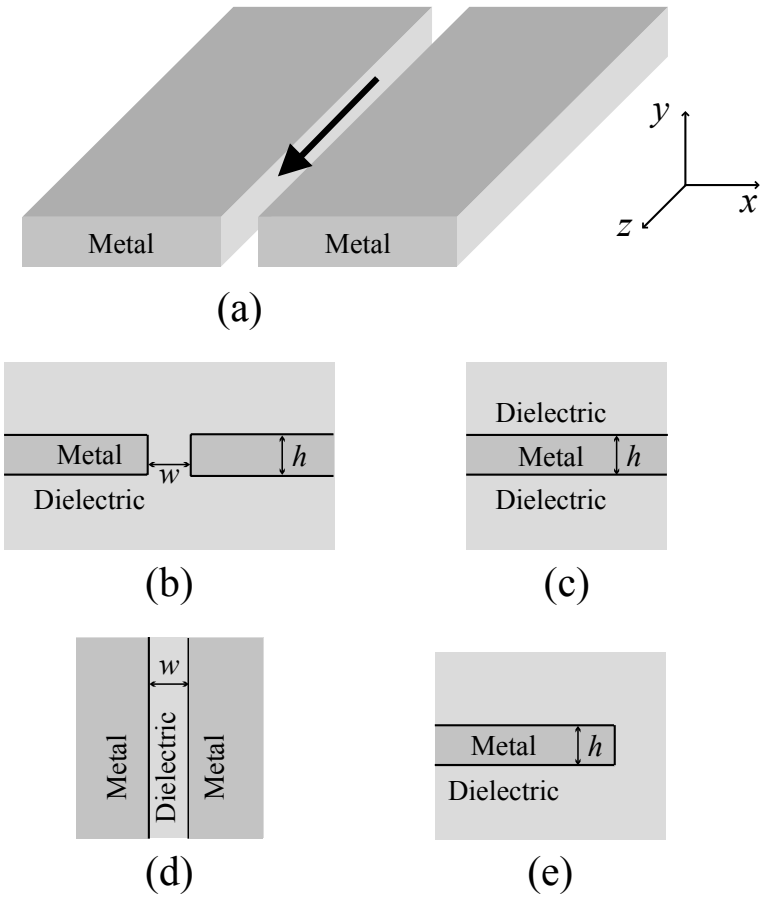

Figure 1. (a) Geometry of a 3D plasmonic slot waveguide. The arrow shows the direction of propagation of the optical mode. (b) Cross-sectional view of the 3D plasmonic slot waveguide geometry. (c)-(e) Corresponding IMI, MIM, and truncated metal film structures for the 3D plasmonic slot waveguide of Figure 1b.

and optoelectronic devices. The characteristics of the modes supported by plasmonic slot waveguides at visible wavelengths (λ_0 =632.8 nm) have also been investigated.[17,18]

In this paper we investigate in detail the characteristics of the modes supported by 3D plasmonic slot waveguides. In particular, we illustrate the physics of such a waveguide by comparing it to a number of simplified geometries shown in Figure 1c-e. We first consider a reference symmetric plasmonic slot waveguide structure, comprised of a slot in a thin metallic film embedded in an infinite homogeneous dielectric. We show that the fundamental mode supported by this symmetric plasmonic slot waveguide is always a bound mode for any combination of operating wavelength and waveguide parameters. We then consider an asymmetric plasmonic slot waveguide structure in which the surrounding dielectric media above and below the metal film are different. Unlike the symmetric case, in the asymmetric case the fundamental propagating mode is not always bound. We show that for a specific asymmetric plasmonic slot waveguide there may exist a cutoff slot width and/or a cutoff metal film thickness above which the mode becomes leaky, and there always exists a cutoff wavelength above which the mode becomes leaky.

2. SIMULATION METHOD

We calculate the eigenmodes of plasmonic waveguides at a given wavelength λ_0 using a full-vectorial finite-difference frequency-domain (FDFD) mode solver.[16,23] For waveguiding structures which are uniform in the z direction, if an $\exp(-\gamma z)$ dependence is assumed for all field components, Maxwell's equations reduce to two coupled equations for the transverse magnetic field components H_x and H_y[23]

$$-\epsilon_r k_0^2 h_x + \epsilon_r \frac{\partial}{\partial y}[\epsilon_r^{-1}(\frac{\partial h_y}{\partial x} - \frac{\partial h_x}{\partial y})] - \frac{\partial}{\partial x}(\frac{\partial h_x}{\partial x} + \frac{\partial h_y}{\partial y}) = \gamma^2 h_x$$

$$-\epsilon_r k_0^2 h_y - \epsilon_r \frac{\partial}{\partial x}[\epsilon_r^{-1}(\frac{\partial h_y}{\partial x} - \frac{\partial h_x}{\partial y})] - \frac{\partial}{\partial y}(\frac{\partial h_x}{\partial x} + \frac{\partial h_y}{\partial y}) = \gamma^2 h_y$$

where $\mathbf{H}(x,y,z) = \mathbf{h}(x,y)\exp(-\gamma z)$, $\epsilon_r = \epsilon_r(x,y)$ is the dielectric function, and $k_0^2 = \omega^2\epsilon_0\mu_0$. Solving these eigenvalue equations allows one to define the propagation length L_p and the effective index n_eff of a propagating mode through the equation $\gamma \equiv L_\mathrm{p}^{-1} + i\beta = L_\mathrm{p}^{-1} + i2\pi n_\mathrm{eff}\lambda_0^{-1}$. Also, the dispersion relation is defined as $\omega = \omega(\beta)$. These equations are discretized on a non-uniform orthogonal grid resulting in a sparse matrix eigenvalue problem of the form $\mathbf{Ah} = \gamma^2\mathbf{h}$, which is solved using iterative sparse eigenvalue techniques.[24] The discretization scheme is based on Yee's lattice.[23] To calculate the bound eigenmodes of the waveguide, we ensure that the size of the computational domain is large enough so that the fields are negligibly small at its boundaries,[25] while for leaky modes we use perfectly matched layer (PML) absorbing boundary conditions.[24] An important feature of this formulation is the absence of spurious modes.[25] In addition, metals have complicated dispersion properties in the optical wavelength range. As an example, Figure 2 shows the real and imaginary part of the dielectric constant of silver at optical frequencies.[12,26] The frequency-domain mode solver allows us to directly use experimental data for the frequency-dependent dielectric constant of metals, including both the real and imaginary parts, with no approximation.

3. SIMPLIFIED PLASMONIC STRUCTURES

In order to understand the modal structure of the slot waveguide shown in Figure 1a and b, we first consider the modes in corresponding simplified geometries that include two-dimensional (2D) insulator-metal-insulator (IMI) (Figure 1c), and metal-insulator-metal (MIM) (Figure 1d) plasmonic waveguiding structures, as well as the edge on a truncated metal film (Figure 1e). The asymptotic behavior of many properties of 3D plasmonic slot waveguides can be explained in terms of the properties of these simpler plasmonic structures. Below we focus only on those modes in these simplified structures which are directly related to the fundamental modes of the slot.

The corresponding IMI plasmonic structure (Figure 1c) has the same metal film thickness as the film in the slot waveguide (Figure 1b). Such a structure supports two modes below the surface plasmon frequency.[11] Of relevance here is the higher-index mode, which is conventionally called short-range SPP (SR-SPP), that has

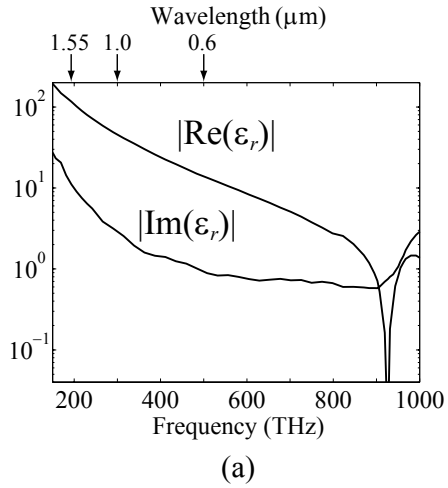

λ (μm)	$\mathrm{Re}(\varepsilon_r)$	$\mathrm{Im}(\varepsilon_r)$
1.55	−143	−10
1.0	−53	−4
0.6	−16	−2

(b)

Figure 2. (a) Absolute values of the real ($\Re(\epsilon_r)$) and imaginary ($\Im(\epsilon_r)$) part of the dielectric constant of silver at optical frequencies. $\Re(\epsilon_r) < 0$ for frequencies below ∼910 THz. (b) The dielectric constant of silver at selected wavelengths.

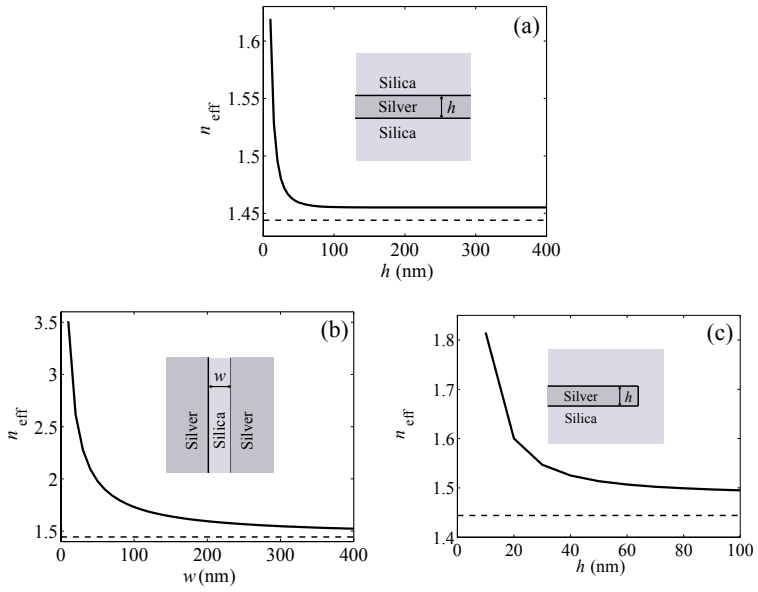

Figure 3. (a) The effective index n_{eff} of the SR-SPP of a silica-silver-silica IMI structure (see inset) as a function of the width of the central silver region h (solid line). We also show the refractive index of silica (dashed line). (b) The effective index n_{eff} of the G-SPP of a silver-silica-silver MIM structure (see inset) as a function of the width of the central silica region w (solid line). We also show the refractive index of silica (dashed line). (c) The effective index n_{eff} of the fundamental edge mode of a truncated silver film embedded in silica as a function of the metal film thickness h (solid line). We also show the refractive index of silica (dashed line).

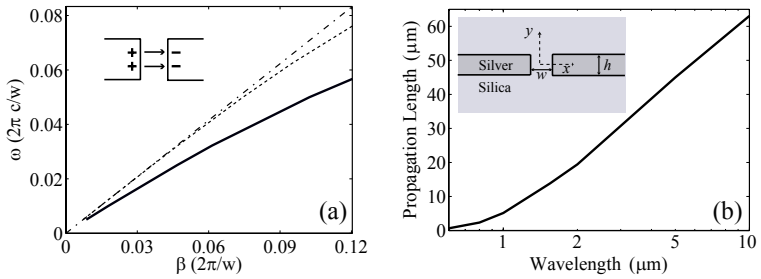

Figure 4. (a) Dispersion relation of the fundamental mode of the symmetric plasmonic slot waveguide (shown with solid line) for w, h =50 nm (see inset of Figure 4b). The inset shows a schematic of the charge and vector field distribution of the mode. The dash-dotted line is the light line of silica, while the dashed curve is the dispersion relation of the SR-SPP in the silica-silver-silica IMI thin film structure. (b) Propagation length of the fundamental mode of the symmetric plasmonic slot waveguide as a function of wavelength for w, h =50 nm.

symmetric charge distribution. In Figure 3a we show the effective index n_{eff} of the SR-SPP of a silica-silver-silica IMI structure as a function of the width of the central silver region h. As a somewhat unusual feature, when h decreases, the fraction of the modal power in the metal increases, and n_{eff} therefore increases. In the opposite limit, as $h \to \infty$, the coupling between the surface plasmon modes of the two metal-dielectric interfaces vanishes, and n_{eff} therefore approaches asymptotically the effective index of the surface plasmon mode of a single metal-dielectric interface.

The corresponding MIM plasmonic structure (Figure 1d) has a dielectric film thickness equal to the slot width (Figure 1b). Such a structure supports a fundamental mode, the so called gap SPP (G-SPP), below the surface plasmon frequency with antisymmetric charge distribution.[11] In Figure 3b we show the effective index n_{eff} of the G-SPP of a silver-silica-silver MIM structure as a function of the width of the central silica region w. As w decreases, the fraction of the modal power in the metal increases, and n_{eff} therefore increases. In the opposite limit, as $w \to \infty$, n_{eff} approaches asymptotically the effective index of the surface plasmon mode of a single metal-dielectric interface, as in the IMI structure. We also note that for a given width of the central region the coupling of the single-interface surface plasmon modes is substantially stronger in the MIM case compared to the IMI case, since in the former case the coupling occurs through dielectric, while in the latter it occurs through metal.

The corresponding truncated metal film structure (Figure 1e) has the same metal film thickness as the film in the slot waveguide (Figure 1b). Such a structure supports a fundamental edge mode. In Figure 3c we show the effective index n_{eff} of the fundamental edge mode of a truncated silver film embedded in silica as a function of the metal film thickness h (solid line). Similar to the IMI structure, n_{eff} increases, as h decreases. In the opposite limit, as $h \to \infty$, n_{eff} approaches asymptotically the effective index of the mode of a single 90° corner, which is higher than the effective index of a single-interface surface plasmon mode.[27]

4. SYMMETRIC PLASMONIC SLOT WAVEGUIDE

We now consider a symmetric plasmonic slot waveguide structure comprised of a slot in a thin metallic film embedded in an infinite homogeneous dielectric. We are particularly interested in the regime where the dimensions of the slot are much smaller than the wavelength of light. Thus, our reference structure consists of a slot of width w =50 nm in a silver film of thickness h =50 nm embedded in silica (n_{s} =1.44) (inset of Figure 4b).

In Figure 4a we show the dispersion relation of the fundamental mode supported by our reference structure. We observe that the fundamental mode of the plasmonic slot waveguide has a wavevector larger than all radiation modes in silica, as well as all propagating modes in the silica-silver-silica IMI thin film structure over the entire frequency range. The fundamental mode supported by our reference plasmonic slot waveguide is therefore a

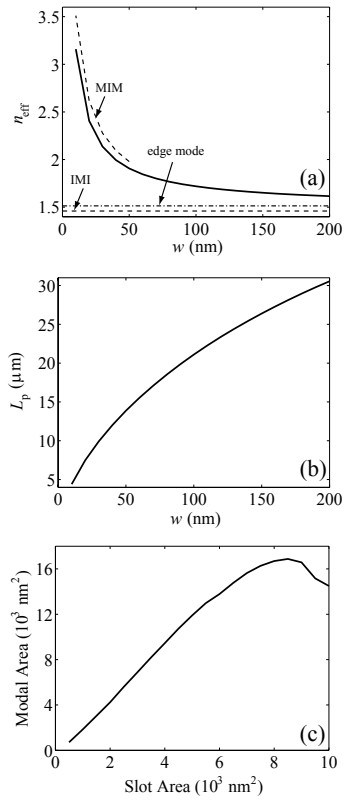

Figure 5. (a) The effective index $n_{\rm eff}$ of the fundamental mode of the symmetric plasmonic slot waveguide (solid line) as a function of the slot width w (Figure 4b). We also show the effective index of the G-SPP of the corresponding MIM structure (dashed line); the effective index of the SR-SPP of the corresponding IMI structure (dashed line); the effective index of the edge mode of the corresponding truncated metallic film (dash-dotted line). (b) The propagation length $L_{\rm p}$ of the fundamental mode of the symmetric plasmonic slot waveguide as a function of the slot width w (Figure 4b). (c) The modal area of the fundamental mode of the symmetric plasmonic slot waveguide as a function of the slot area $w \times h$, as w is varied (Figure 4b). All other parameters are as in our reference structure (Figure4).

bound mode. Since the slot dimensions are much smaller than the wavelength in the frequency range of interest, this waveguide does not support any higher order propagating bound modes.

In Figure 4b we show the propagation length $L_{\rm p}$ of the fundamental mode of our reference plasmonic slot waveguide as a function of wavelength. The propagation length decreases as the wavelength decreases. This is consistent with the behavior of plasmonic structures in general,[1] since the fraction of the modal power in the metal increases at shorter wavelengths.

In the remainder of this section, we investigate the effect of variations of the parameters of our reference plasmonic slot waveguide structure on the modal characteristics. We focus on the optical communication wavelength (λ_0 =1.55 μm) where subwavelength plasmonic slot waveguides have propagation lengths of tens of micrometers.[16]

In Figure 5a,b we show, respectively, the effective index $n_{\rm eff}$, and propagation length $L_{\rm p}$ of the fundamental mode of the plasmonic slot waveguide as a function of the slot width w (Figure 4b). All other parameters are as in our reference structure (Figure 4). We observe that as w decreases, $n_{\rm eff}$ increases, and $L_{\rm p}$ decreases. This is due to the fact that as w decreases, the fraction of the modal power in the metal increases. Similar behavior is observed in MIM plasmonic waveguides.[7,13,14] In fact for $w \to 0$ we observe that $n_{\rm eff}(w)$ is very close to $n_{\rm eff}(w)|_{\rm MIM}$ (Figure 5a). In the limit of $w \to \infty$, $n_{\rm eff}(w)$ approaches asymptotically the effective index of the edge mode (shown with the dash-dotted line in Figure 5a), which is slightly higher than the effective index of the SR-SPP of the corresponding IMI structure[11] (shown with the dashed line in Figure 5a). The same asymptotic

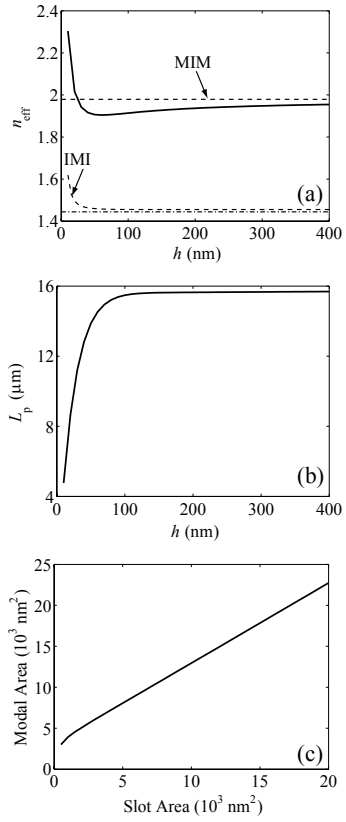

Figure 6. (a) The effective index $n_{\rm eff}$ of the fundamental mode of the symmetric plasmonic slot waveguide (solid line) as a function of the thickness h of the metallic film (Figure 4b). We also show the effective index of the G-SPP of the corresponding MIM structure (dashed line); the effective index of the SR-SPP of the corresponding IMI structure (dashed line); the refractive index of the substrate (dash-dotted line). (b) The propagation length $L_{\rm p}$ of the fundamental mode of the symmetric plasmonic slot waveguide as a function of the thickness h of the metallic film (Figure 4b). (c) The modal area of the fundamental mode of the symmetric plasmonic slot waveguide as a function of the slot area $w \times h$, as h is varied (Figure 4b). All other parameters are as in our reference structure (Figure 4).

behaviors are also observed in the propagation length $L_{\rm p}(w)$ for $w \to 0$ and $w \to \infty$. In Figure 5c we show the modal area (defined as the area in which the mode power density is larger than $1/e^2$ of its maximum value) of the fundamental mode of the plasmonic slot waveguide as a function of the slot area $w \times h$, as w is varied (Figure 4b). As expected, for small w the modal area increases, as w increases. In addition, the coupling between the edge modes of the two semi-infinite metal film regions which form the slot decreases, as w increases. Therefore, when w is larger than the decay length of the edge mode in silica, the modal area decreases, as w increases. As $w \to \infty$, the modal area asymptotically approaches twice the area of the edge mode.

In Figure 6a,b we show, respectively, the effective index $n_{\rm eff}$, and propagation length $L_{\rm p}$ of the fundamental mode of the plasmonic slot waveguide as a function of the thickness h of the metallic film (Figure 4b). All other parameters are as in our reference structure (Figure 4). As $h \to \infty$, the effective index of the mode approaches asymptotically the effective index of the G-SPP of the corresponding MIM plasmonic waveguide ($\lim_{h\to\infty} n_{\rm eff}(h) = n_{\rm eff}|_{\rm MIM}$), and the same asymptotic behavior is observed in the propagation length $L_{\rm p}(h)$. In Figure 6c we show the modal area of the fundamental mode of the plasmonic slot waveguide as a function of the slot area $w \times h$, as h is varied (Figure 4b). The modal area increases, as h increases, and for large h the increase is linear.

We also observe that as $h \to 0$, $n_{\rm eff}(h)$ increases, and $L_{\rm p}(h)$ decreases. We found that this behavior is related to the fringing fields of the mode rather than the fields in the slot region. The dominant components of the

fringing fields are E_y and H_x, and they are maximum at the four lateral silver-silica interfaces at $y = \pm h/2$, $x > w/2$ or $x < -w/2$ (inset of Figure 4b). As the film thickness h decreases, the fraction of modal power in the metal at these interfaces increases, and this results in increasing effective index n_{eff} and decreasing propagation length L_{p}. The same trend is also observed at visible wavelengths.[18] We also observe that in the limit of $h \to 0$ the modal area approaches an asymptotic non-zero value (Figure 6c), unlike the $w \to 0$ case. In other words, there is a minimum modal size as the film thickness approaches zero due to the fringing fields of the mode.

We also investigated the effect of varying the dielectric constant of the medium in which the metallic film with the slot is embedded. We found that as the permittivity of the dielectric is increased, the effective index n_{eff} of the fundamental mode increases, and its propagation length L_{p} decreases. As in the case of a single-interface surface-plasmon mode,[1] this is due in part to increased fraction of modal power in the metal as the permittivity of the dielectric increases, as well as decreased group velocity. Finally, we note that in the case of the symmetric plasmonic slot waveguide the wavevector of the fundamental mode is larger than all radiation modes in the surrounding dielectric, as well as all propagating modes in the corresponding IMI thin film structure (Figure 1c), for any combination of operating wavelength and waveguide parameters. In other words, in the symmetric plasmonic slot waveguide there always exists a fundamental propagating bound mode, and there is no associated cutoff.

5. ASYMMETRIC PLASMONIC SLOT WAVEGUIDE

We now consider an asymmetric plasmonic slot waveguide structure in which the surrounding dielectric media above and below the metal film are different. More specifically, we consider a waveguide consisting of an air slot of width w in a metallic film of thickness h deposited on silica (inset of Figure 7a).

In Figure 7a,b we show, respectively, the effective index n_{eff}, and propagation length L_{p} of the fundamental mode of the asymmetric plasmonic slot waveguide as a function of the slot width w (inset of Figure 7a). All other parameters are as in our reference structure (Figure 4). In Figure 7c we show the modal area of the fundamental mode of the asymmetric plasmonic slot waveguide as a function of the slot area $w \times h$, as w is varied. We observe that in general the effect of variation of the slot width w on the characteristics of the fundamental mode supported by the plasmonic slot waveguide is very similar in both the symmetric (Figure 5) and asymmetric (Figure 7) cases. However, there is an important difference between the two cases regarding the asymptotic behavior for $w \to \infty$. Unlike the symmetric case, in the asymmetric case the fundamental propagating mode is not always bound. If all other waveguide parameters are fixed, there is a slot width cutoff w_{cutoff}, and for $w > w_{\text{cutoff}}$ the mode is leaky. More specifically, we observe that if w is gradually increased to be w_{cutoff}, the modal power starts to leak into the propagating modes of the IMI air-silver-silica thin film structure, and if w is further increased so that $w > w_{\text{cutoff,substrate}}$, the modal power also leaks into the radiation modes in the silica substrate (Figure 7a). In general as $w \to \infty$, $n_{\text{eff}}(w)$ approaches asymptotically the effective index of the edge mode of a truncated metal film deposited on the substrate. For the structure shown in the inset of Figure 7a the effective index of the edge mode is smaller than the effective index of the SR-SPP of the asymmetric IMI (air-silver-silica) structure. Hence there exists a cutoff width w_{cutoff}. In addition, the effective index of the edge mode is also smaller than the refractive index of the substrate (silica in Figure 7). Hence there also exists a cutoff width $w_{\text{cutoff,substrate}}$. We also observe that the propagation length L_{p} of the fundamental mode of the asymmetric plasmonic slot waveguide increases with w, even when the mode becomes leaky. This indicates that the dominant loss mechanism is the material loss in the metal. As w increases, the mode becomes less confined, and the power loss in the metal decreases. Thus, even though the radiation power loss increases with w, the overall power loss decreases. In fact, for $w > w_{\text{cutoff}}$ in the asymmetric case (Figure 7b) the propagation length L_{p} increases more rapidly with w compared to the symmetric case (Figure 5b), because leakage further reduces the mode confinement and therefore the power loss in the metal.

In Figure 8a,b we show, respectively, the effective index n_{eff}, and propagation length L_{p} of the fundamental mode of the asymmetric plasmonic slot waveguide as a function of the metallic film thickness h (inset of Figure 7a). All other parameters are as in our reference structure (Figure 4). In Figure 8c we show the modal area of the fundamental mode of the asymmetric plasmonic slot waveguide as a function of the slot area $w \times h$, as h is varied. As in the case of slot width w variation (Figure 5 and Figure 7), we observe that in general the effect of metallic film thickness h variation on the characteristics of the fundamental mode supported by the plasmonic

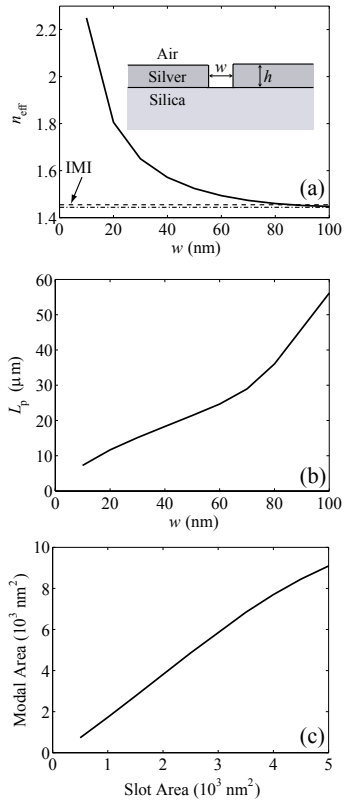

Figure 7. (a) The effective index n_{eff} of the fundamental mode of the asymmetric plasmonic slot waveguide (solid line) as a function of the slot width w (see inset). We also show the effective index of the SR-SPP of the corresponding asymmetric IMI structure (dashed line); the refractive index of the substrate (dash-dotted line). (b) The propagation length L_{p} of the fundamental mode of the asymmetric plasmonic slot waveguide as a function of the slot width w (Figure 7a). (c) The modal area of the fundamental mode of the asymmetric plasmonic slot waveguide as a function of the slot area $w \times h$, as w is varied (Figure 7a). All other parameters are as in our reference structure (Figure 4).

slot waveguide is very similar in both the symmetric (Figure 6) and asymmetric (Figure 8) cases. The most important difference between the two cases is related to the asymptotic behavior for $h \to \infty$. In the asymmetric case, as $h \to \infty$, the effective index of the fundamental mode $n_{\text{eff}}(h)$ approaches asymptotically the effective index of the G-SPP of the MIM plasmonic waveguide with dielectric core corresponding to the dielectric media in the slot. Since, for the structure shown in Figure 7, the effective index of the G-SPP supported by this MIM structure (silver-air-silver in Figure 7) is smaller than the effective index of the SR-SPP of the asymmetric IMI structure (air-silver-silica in Figure 7), there exists a cutoff film thickness h_{cutoff}. For $h > h_{\text{cutoff}}$ there is no longer a fundamental guided mode. In addition, for this structure, since the G-SPP mode effective index of the MIM (silver-air-silver in Figure 7) is smaller than the refractive index of the substrate (silica in Figure 7), there also exists a cutoff film thickness due to the substrate $h_{\text{cutoff,substrate}}$ above which the fundamental mode leaks into the substrate. We also observe that the propagation length L_{p} of the fundamental mode of the asymmetric plasmonic slot waveguide increases with h, even when the mode becomes leaky (Figure 8b), for similar reasons as those mentioned above for the case of increasing w.

As mentioned above, the cutoff slot width depends on the effective index of the corresponding edge mode. Similarly, the cutoff film thickness depends on the G-SPP mode effective index of the corresponding MIM plasmonic waveguide with dielectric core corresponding to the dielectric media in the slot. Therefore, the structure will not have a cutoff slot width or film thickness for the fundamental mode, if the slot is filled with the same dielectric as the substrate. We note however that for any asymmetric plasmonic slot waveguide there always exists a cutoff wavelength above which the mode becomes leaky. This is due to the fact that in the long

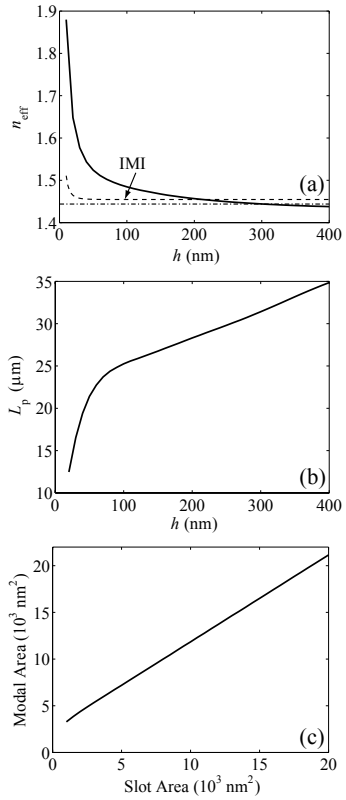

Figure 8. (a) The effective index n_{eff} of the fundamental mode of the asymmetric plasmonic slot waveguide (solid line) as a function of the thickness h of the metallic film (Figure 7a). We also show the effective index of the SR-SPP of the corresponding asymmetric IMI structure (dashed line); the refractive index of the substrate (dash-dotted line). (b) The propagation length L_{p} of the fundamental mode of the asymmetric plasmonic slot waveguide as a function of the thickness h of the metallic film (Figure 7a). (c) The modal area of the fundamental mode of the asymmetric plasmonic slot waveguide as a function of the slot area $w \times h$, as h is varied (Figure 7a). All other parameters are as in our reference structure (Figure 4).

wavelength limit metals behave as perfect electric conductors, so that the modal fields do not penetrate into the metal. Since some of the field lines are in the upper and some are in the lower dielectric media, the effective index of the mode always lies between the refractive indices of the upper and lower dielectric media, and the mode is therefore always leaky.[16] Finally, we note that as the structure becomes more asymmetric, the cutoff slot width, cutoff film thickness, and cutoff wavelength decrease.

ACKNOWLEDGMENTS

This research was supported by DARPA/MARCO under the Interconnect Focus Center and by AFOSR grant FA 9550-04-1-0437.

REFERENCES

1. W. L. Barnes, A. Dereux, and T. W. Ebbesen *Nature* **424**, pp. 824–830, 2003.
2. J. Takahara, S. Yamagishi, H. Taki, A. Morimoto, and T. Kobayashi *Opt. Lett.* **22**, pp. 475–477, 1997.
3. J. C. Weeber, A. Dereux, C. Girard, J. R. Krenn, and J. P. Goudonnet *Phys. Rev. B* **60**, pp. 9061–9068, 1999.
4. J. R. Krenn, B. Lamprecht, H. Ditlbacher, G. Schider, M. Salerno, A. Leitner, and F. R. Aussenegg *Europhys. Lett.* **60**, pp. 663–669, 2002.
5. M. L. Brongersma, J. W. Hartman, and H. A. Atwater *Phys. Rev. B* **62**, pp. R16356–R16359, 2000.
6. S. A. Maier, P. G. Kik, H. A. Atwater, S. Meltzer, E. Harel, B. E. Koel, and A. A. G. Requicha *Nat. Mater.* **2**, pp. 229–232, 2003.
7. S. I. Bozhevolnyi, V. S. Volkov, E. Devaux, and T. W. Ebbesen *Phys. Rev. Lett.* **95**, p. 046802, 2005.
8. S. I. Bozhevolnyi, V. S. Volkov, E. Devaux, J. Y. Laluet, and T. W. Ebbesen *Nature* **440**, pp. 508–511, 2006.
9. E. Feigenbaum and M. Orenstein *J. Lightwave Technol.* **25**, pp. 2547–2562, 2007.
10. D. M. Pozar, *Microwave Engineering*, Wiley, New York, 1998.
11. E. N. Economou *Phys. Rev.* **182**, pp. 539–554, 1969.
12. E. D. Palik, *Handbook of Optical Constants of Solids*, Academic, New York, 1985.
13. R. Zia, M. D. Selker, P. B. Catrysse, and M. L. Brongersma *J. Opt. Soc. Am. A* **21**, pp. 2442–2446, 2004.
14. K. Tanaka and M. Tanaka *Appl. Phys. Lett.* **82**, pp. 1158–1160, 2003.
15. F. Kusunoki, T. Yotsuya, J. Takahara, and T. Kobayashi *Appl. Phys. Lett.* **86**, p. 211101, 2005.
16. G. Veronis and S. Fan *Opt. Lett.* **30**, pp. 3359–3361, 2005.
17. L. Liu, Z. Han, and S. He *Opt. Express* **13**, pp. 6645–6650, 2005.
18. D. F. P. Pile, T. Ogawa, D. K. Gramotnev, Y. Matsuzaki, K. C. Vernon, K. Yamaguchi, T. Okamoto, M. Haraguchi, and M. Fukui *Appl. Phys. Lett.* **87**, p. 261114, 2005.
19. J. A. Dionne, H. J. Lezec, and H. A. Atwater *Nano Lett.* **6**, pp. 1928–1932, 2006.
20. L. Chen, J. Shakya, and M. Lipson *Opt. Lett.* **31**, pp. 2133–2135, 2006.
21. G. Veronis and S. Fan *J. Lightwave Technol.* **25**, pp. 2511–2521, 2007.
22. N. N. Feng, M. L. Brongersma, and L. D. Negro *IEEE J. Quantum Electron.* **43**, pp. 479–485, 2007.
23. J. A. Pereda, A. Vegas, and A. Prieto *Microwave Opt. Tech. Lett.* **38**, pp. 331–335, 2003.
24. J. Jin, *The Finite Element Method in Electromagnetics*, Wiley, New York, 2002.
25. S. J. Al-Bader *IEEE J. Quantum Electron.* **40**, pp. 325–329, 2004.
26. H. J. Hagemann, W. Gudat, and C. Kunz *J. Opt. Soc. Am.* **65**, pp. 742–744, 1975.
27. D. F. P. Pile, T. Ogawa, D. K. Gramotnev, T. Okamoto, M. Haraguchi, M. Fukui, and S. Matsuo *Appl. Phys. Lett.* **87**, p. 061106, 2005.